



Properties of Contaminated Reinforced Concrete Added by *Areca catechu* Leaf Extract as an Eco-friendly Corrosion Inhibitor

Syedmojtaba Ghoreishiamiri¹ · Pandian Bothi Raja² · Mohammad Ismail¹ · Seyedeh Faezeh Hashemi Karouei³

Received: 13 July 2020 / Revised: 30 August 2020 / Accepted: 29 September 2020 / Published online: 7 October 2020
© Springer Nature Switzerland AG 2020

Abstract

The main reason causing the degeneration of steel-reinforced concrete is supposed to be corrosion of reinforcement steel. In this study, electrochemical impedance spectroscopy (EIS), linear polarization resistance (LPR), and weight loss have been utilized to evaluate the corrosion of steel reinforcement in contaminated, chemical inhibitor (sodium nitrite) and green inhibitor (*Areca catechu* extract)-added concrete. Besides, ultrasonic pulse velocity, sulfate and acid attack resistance, heat of hydration, and specific heat capacity tests have been performed to investigate the effect of inhibitor addition on permeability and durability of corrosion inhibitor-added samples. The concrete contaminated with 5% of Magnesium Sulfate ($MgSO_4$) and Sodium Chloride (NaCl) as corrosion stimulant. The results showed that *Areca catechu* was more corrosive than sodium nitrite. Further, there was no gypsum found visible in SEM observation for *Areca catechu*-added concrete. The green and chemical inhibitor-modified samples could improve the specific heat capacity behavior of contaminated concrete by 10.77% and 13.25%, respectively. *Areca catechu* could decrease the corrosion rate of contaminated concrete about 30%, even in an extreme harsh environment applied in the current study. Polarization analysis depicted that *Areca catechu* extract acted as a mixed-type inhibitor.

Keywords Corrosion · Green corrosion inhibitors · Weight loss · Contamination · Concrete properties

1 Introduction

One of the most significant types of damage that occurs in existing impaired reinforced concrete structures is the corrosion of reinforcing bars embedded in reinforced concrete. Chloride ion (Cl^-) and carbon dioxide (CO_2) penetration from the corrosive environment could disrupt passivity

conditions provided by the surrounding concrete to the reinforcing bar [1]. Since high-quality concrete offers chemical and physical conservation to the steel reinforcement bars, the risk of corrosion is supposed to be negligible. When corrosion starts, volumetric expansion of the rust around the reinforcing bars against the surrounding concrete might be a result of active corrosion [2–4]. The corrosion of reinforcing bars in concrete is mostly assumed as an electrochemical process [5, 6]. Severe corrosion could occur by interfacing between harmful ions (like chlorides and sulfates) and the steel reinforcement, which may threaten the whole structure [7–9]. Using chemical admixtures as corrosion inhibitors is an appropriate method to prevent and delay the corrosion of rebar. A perfect corrosion inhibitor is defined as an admixture that can prevent corrosion of reinforcing steel in concrete when added in suitable amounts [10, 11]. Some of the advantages of inhibitors utilization are being simple to apply, decreasing the corrosion rate of different steel structures in the corrosive mediums without interfering to the process. Inorganic (majorly nitrites) and organic corrosion inhibitors (alkanolamine and their inorganic, organic acid salt mixtures) are two main classifications of corrosion

✉ Syedmojtaba Ghoreishiamiri
mojtaba.ghoreishi@gmail.com

Pandian Bothi Raja
bothiraja@gmail.com

Mohammad Ismail
mohammad@utm.my

Seyedeh Faezeh Hashemi Karouei
seidehfaezeh_hashemi@yahoo.com

¹ Faculty of Civil Engineering, Universiti Teknologi Malaysia, 81310 UTM Johor Bahru, Johor, Malaysia

² School of Chemical Sciences, Universiti Sains Malaysia, 11800 Penang, Malaysia

³ Department of Solid State Physics, University of Mazandaran, 4741695447 Babolsar, Iran

inhibitors used for concrete [12–15]. Due to their protection mechanisms, they supposed to be categorized as an anodic, cathodic, and mixed inhibitor. There are two main types of inhibitor utilization, which are; application into reinforced concrete either as a preventive agent to a new structure or as surface applied component for preventive and conservative goals [16]. Regarding the mode of inhibitor's applications, they can be categorized as migrating inhibitors and admixed inhibitors [17–21]. Utilization of many inhibitors is mostly hindered since they are toxic and lethal to both environment and living creatures. Thus, effective and non-toxic inhibitors are widely paid attention due to amplified environmental risks and awareness of health [22–25]. Presence of heteroatoms like oxygen, nitrogen, sulfur, and several bonds in their molecules responsible for the effective adsorption on the metal surface, organic compounds are supposed to be used in the near future [26–30]. Besides, green corrosion inhibitors are cheaper, less toxic, and more eco-friendly when compared with chemical inhibitors. Many kinds of research focused on the effects of corrosion on bond behavior, the change in mechanical properties, and other issues which are related to corrosion [31–34]. There is a lack of research on natural corrosion circumstances due to existing complexities, since most present studies were conducted under accelerated corrosion conditions. One of the agricultural waste products dumped in the environment as land filler is *Areca catechu* leaf residue. Production of useful industrial products that could be utilized in concrete constructions from waste materials might have beneficial impacts on the economy.

Corrosion of reinforced concrete structures and its detrimental effect enforce worries to many countries around the world. Hence, discovering the advantages of inhibitor usage is very prominent. Recognition of inhibitor's effect on concrete properties could be the second step for utilization of inhibitors in concrete structures. Actually, they can preserve, improve, or even worsen the concrete properties. The current research aims to produce economic concrete structures in industrial scale without concerning the side effects of corrosion. Moreover, the current study could reduce the financial indemnity affect by corrosion consequently. Employing environment-friendly and non-toxic inhibitor to avoid the environment pollution which is made by means of toxic chemical inhibitors, improvement of concrete behaviors due to corrosion, reducing the cost of concrete structures during their life cycle, and increasing the life-time of reinforced concrete structures could be other primary outcomes of recent research. Current research findings will contribute towards the application of *Areca catechu* as green corrosion inhibitor which has never been used before for corrosion inhibition of reinforcement in concrete to preserve the concrete properties while reducing the corrosion rate simultaneously.

The use of dried leaf of *Areca catechu* as waste products in the field of corrosion science of reinforced concrete structures has not been recognized yet. High amount of electrons in molecules such as lignin, ursolic acid, cellulose, 3b acetyl ursolic acid, and hemicelluloses are reported to be found in *Areca catechu* leaf extract [35]. There is a scarcity of academic studies on corrosion inhibition property of *Areca catechu* leaf extract for reinforcement embedded in reinforced concrete curing in corrosive mediums. Hence, *Areca catechu* leaf extract is selected in the present study for investigating the inhibition of reinforcing bar in contaminated reinforced concrete in an aggressive medium. The standard corrosion tests such as potentiodynamic polarization (Tafel curves), impedance techniques, and gravimetric (mass loss) were employed to investigate the corrosion inhibition potential of *Areca catechu* leaf extract. Moreover, scanning electron microscopy (SEM) and energy dispersive X-ray spectroscopy (EDX) tool were employed to deep-screen the reinforcement steel morphology in the presence and absence of *Areca catechu* leaf extract. In addition, ultrasonic pulse velocity, specific heat capacity, heat of hydration, sulfate resistance, and acid attack resistance tests were performed to evaluate the durability and permeability of contaminated concrete samples added by novel green inhibitor.

2 Experimental Details

Areca catechu extract was employed as green corrosion inhibitor for reinforcement steel in concrete, which has been analyzed through electrochemical, gravimetric, and microstructural analyses of ordinary portland concrete, contaminated concrete, and modified contaminated concrete with chemical and green inhibitors added.

2.1 Plant Extraction Procedure

Areca catechu leaf were collected from local palm oil tree farms, shade dried at room temperature after washing in tap water. Afterward, 15 g of leaves was ground and placed in a porous cellulose thimble. Ethanol was employed as a solvent and heated up to 75 °C (below the boiling point of ethanol) in the lower flask. The extraction procedure followed up the soxhlet extraction method as well. At the end of 6 h of extraction, the resultant extract was removed from the flask. Normal filter paper was used to remove impurities and small solid particles of plant leaves and the residual ethanol was evaporated using rotatory evaporator.

2.2 Composition of *Areca catechu* leaf

Phytochemical analysis on *Areca catechu* leaf extract was carried out to find out the active constituents and also atomic absorption spectroscopy (AAS) analysis to discover alkali metals present in the plant extract.

2.3 Concrete Mix Design and Molding

The mix design specified as OPC is the control batch. MN5C is associated with the batch contaminated with 5% Magnesium Sulfate ($MgSO_4$) and Sodium Chloride (NaCl). CI2C represents the contaminated batch added with 2% (optimum percentage) of sodium nitrite ($NaNO_2$). GI2C indicates the contaminated batch added with 2% (by the weight of cement) of *Areca catechu* extract. Slab specimens with a size of $200 \times 150 \times 76$ mm were made using wood and a 16-mm mild steel bar embedded in the center of the concrete slab to act as a working electrode. A schematic diagram of the slab specimen is shown in Fig. 1. The procedure for the preparation of steel specimens followed ASTM G109. The samples were demolded 24 h after casting, cured in seawater for 28 days, and then exposed to wet and dry cycles for 360 days [36]. The wet and dry cycles were carried out every week for 360 days.

2.4 Ultrasonic Pulse Velocity (UPV)

Ultrasonic pulse velocity was conducted to check the uniformity in concrete samples. The main idea for the test is to measure the uniformity of concrete and is so efficient in verifying the quality of the material. The experiment was performed based on ASTM C 597-09, (2009) for 7, 28, 89, 180, and 360 days. Pulse velocity was calculated by the formula shown in Eq. (1) described by ASTM C 597-09, (2009). Here, V is ultrasonic pulse velocity (m/s), L is distance between transducers (m), and T is effective time for transit (s).

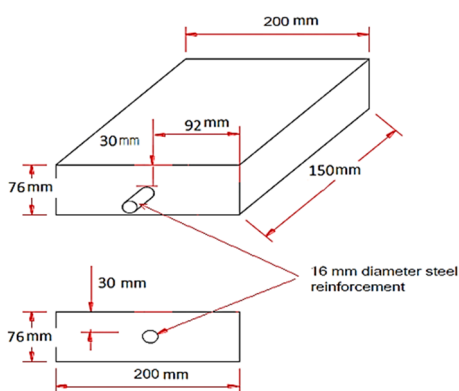


Fig. 1 Slab specimen line diagram in details

$$V = L/T \quad (1)$$

2.5 Specific Heat Capacity

The heat capacity of all modified concrete samples was measured using a similar method for the previous researches for 180 days [37–39]. The interior temperature of the sample was measured using a thermocouple type (K). The samples were weighed to determine initial weight. The water in which the samples were immersed was weighed. The samples were oven dried at $105^\circ C$ for 24 h. Then, the samples were removed from the oven and placed in insulated containers filled with $28^\circ C$ water. Increased water temperatures were recorded at 15-min intervals. The recorded data were used to determine the heat capacity of the concrete using the following Eq. (2):

$$M_1 \times CP_1 \times T_1 = M_2 \times CP_2 \times T_2, \quad (2)$$

where M_1 , M_2 are weight of water and concrete samples; CP_1 , CP_2 are specific heat capacity of water and concrete; and T_1 , T_2 are temperature changes for water and concrete samples, respectively.

2.6 Heat of Hydration

Plywood was cut to make cubical molds with 500 mm sides. The molds were then internally insulated with 76-mm-thick polystyrene. The cubical plywood was used for casting concrete mix of OPC, magnesium sulfate-contaminated samples, and sodium chloride-contaminated samples [40]. The cylindrical samples had a size of 300×150 mm for this test. By inserting a thermocouple type (K) into the center of each box through a hole in the middle of polypropylene foam lid, it connected to an SR1 temperature/humidity digital controller prior to casting, in order to obtain temperature readings. Heat was analyzed using hydration process after pouring the concrete mix into the box. The heat of hydration process was recorded using a data logger with short intervals for the first 24 h and bigger intervals until the temperature decreased to the reference temperature of the concrete. Measurements continued up to 120 h for all mixes [41].

2.7 Sulfate Resistance

The cubical specimens of $100 \times 100 \times 100$ mm were allowed to remain in ordinary water for 28 days and were air-dried for 72 h, before complete immersion in the solution. Cube specimens were wiped and weighed with an electronic weighing balance and this was used as an initial weight for subsequent weight loss calculations. All specimens were submerged in a solution containing a 5%

Na₂SO₄ solution for 7, 28, 89, 180, and 360 days. The solution was replaced regularly every 4 weeks. The reference weight of the specimen and the weight during the immersion period were measured periodically to determine weight loss. The average values of the three specimens were considered for assessment. The deterioration of concrete specimens was studied by measuring the percentage of strength distortion at 7, 28, 89, 180, and 360 days, and was calculated using Eq. (3).

$$\text{SDP} = 100 \times ((F_{\text{cw}} - F_{\text{ca}})/F_{\text{cw}}), \quad (3)$$

where SDP is percentage of strength deterioration, F_{cw} is the average of compressive strength for companion specimen cured in ordinary water, and F_{ca} is the average of compressive strength for the specimen after immersion in sulfate solution.

2.8 Acid Resistance

Concrete cube specimens were directly subjected to an aggressive curing medium of 5% HCl solution after demolding. Prior to immersion, the cube specimens were wiped and weighed to acquire a reference weight. The solution pH was regularly monitored and attuned with the help of pH meter so that the consumed solution could be replaced with fresh solution. The assessment of all types of samples was made based on weight loss and strength deterioration factors. The initial weight of the specimen and weight during the immersion period were periodically measured to determine weight loss. The average values for the three specimens were considered for assessment. Strength deterioration percentage is a quantitative way of expressing the performance of inhibitor-added concrete using qualitative means. The deterioration of concrete specimens was studied by measuring the percentage of strength distortion at 7, 28, 89, 180, and 360 days regarding Eq. 3 similar to Sect. 2.6.

2.9 Corrosion Potential Analysis

Corrosion potential analysis is one of the powerful and convenient techniques to evaluate the corrosion of steel in concrete [18, 42]. In this study, the corrosion of reinforcing steel in concrete was monitored by using VERSASTAT 3. The instrument was adjusted similar to most of the instruments used for corrosion, sensors, and biomedical investigations with a range of ± 650 mA/ ± 10 V as standard for electrochemical applications. Moreover, the frequency range of 10 μ Hz to 1 MHz was considered for an internal frequency response analyzer for impedance analysis provided by VERSASTAT 3.

2.10 Linear Polarization Resistance (LPR)

LPR technique was also conducted with VERSASTAT3 instrument, as similar with EIS method. The corrosion current density (I_{corr}) (A/cm²) was calculated by assuming B as 26 mV. A Stern–Geary eq. was used by [43, 44] to calculate I_{corr} using Eq. (4):

$$I_{\text{corr}} = B/R_p, \quad (4)$$

where B is a constant of a function of the cathodic and anodic Tafel slopes, b_a and b_c as described in Eq. (5),

$$B = b_a \times b_c / (2.303(b_a + b_c)). \quad (5)$$

2.11 Weight Loss

Despite using an independent method for corrosion evaluation assessment and inhibitor screening, weight loss is a standard method to validate the accuracy of other test methods [45]. In order to determine the corrosion rate using weight loss method, the slab specimens were broken at the same ages as the electrochemical analysis tests. The visual observation for corrosion assessment was done for each steel reinforcing bar before cleaning. The corroded steel specimen was cleaned to determine weight loss according to the procedure details stated in ASTM G1 [46]. The solution utilized for cleaning was made by mixing 3.5 g of hexamethylenetetramine and 500 ml of hydrochloric acid and distilled water in order to achieve a volume of 1000 ml. Corrosion rates were calculated using Eq. (6) as given in [46].

$$\text{Cr}(\text{mm}/\text{year}) = (K \times W)/(A \times T \times D), \quad (6)$$

where K is a constant equal to 8.76×10^4 , W is mass loss (grams), A is actual corroded area of steel bar (cm²) after removal from slab specimen and visual observation, T is time of exposure (hours), and D is density of steel equal to 7.85 g/cm³.

2.12 Microstructural Analysis

The concrete morphology and microstructural analysis of steel embedded in concrete were investigated through Field Emission Scanning Electron Microscopy (FESEM). Magnification range was $\times 12$ –900,000 and a working distance of 1–50 mm, depending on working conditions. The nominal resolution is 1.5 nm at 10 kV and WD = 2 mm, while acceleration voltage is 0.1–30 kV. The FESEM device is a GEMINI versatile ultra-high resolution with

Table 1 The results of metals analysis by Atomic absorption Spectroscopy (AAS)

Type of Inhibitor (ppm)	Na	ZN	Mg	Ca	K
<i>Areca catechu</i>	589.1	9.2	586.5	13.1	11,720

a variable pressure solution, equipped with a BRUKER signal processing unit that provided Energy Dispersive X-ray analyzer (EDX).

3 Results and Discussion

The details for results and discussions on the conducted tests are based on the order mentioned in Sect. 2.

3.1 Composition of *Areca catechu* leaf

Preliminary phytochemical screening of the *Areca catechu* leaf extract showed positive results for saponins (Frothing test), tannins (ferric chloride test), flavonoids (with alkaline reagent), and alkaloids (with Dragendorff reagent), which confirmed that resultant extract is a complex mixture. Moreover, Atomic Absorption spectroscopy technique was used to determine the concentration of alkali metals in *Areca catechu* since alkali metals are responsible for inhibition mechanism and maintaining the pH of concrete in the range of 12 to 13 [3]. The high amount of potassium (K⁺) in green inhibitors is clearly derived from Table 1. The formation of a dense gamma ferric oxide that protects steel from corrosion is a result of high level of alkalinity.

3.2 Concrete Quality Investigation

The results of ultrasonic pulse velocity (UPV) of all types of mixes were tested for 7, 28, 89, 180, and 360 days. The UPV values varied in the range of 4013 to 4808 m/s. The range of the values for OPC showed an excellent quality for ordinary concrete mix. It is reported that a UPV value higher 4500 m/s indicates a concrete with excellent quality. The increasing approach of results for OPC could be attributed to the improvement of pore structure of concrete by time regarding the hydration process. The pore structure improves by time due to increased densification of concrete paste which increases with the increase in hydration duration [47]. There is remarkable drop in ultrasonic pulse velocity values after 89 days. It could be attributed to the contamination of magnesium sulfate and sodium chloride added by the mixing water during casting. Magnesium sulfate results in the expansion caused by the formation of expansive salts [48]. Furthermore, the moisture content could be enhanced due to chloride ingress, because of the hygroscopic properties

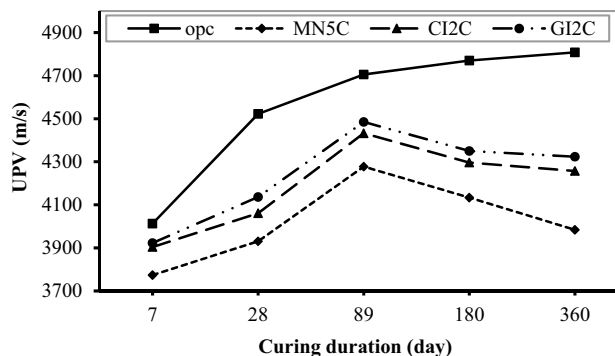


Fig. 2 Ultrasonic pulse velocity approach of all types of mixes

of salts present in concrete, thus increasing the permeability of concrete by time. Additionally, the pH of concrete decreases by the presence of magnesium sulfate and sodium chloride results in more porous concrete. As can be seen in Fig. 2, chemical and green inhibitors improved the value for ultrasonic pulse velocity of the concrete. It might be due to high amount of alkali metals inside the inhibitors resulting in increasing pH of concrete. From the results, *Areca catechu* increased the velocity by 3.95% at 7 days. The respective amounts of increase were 5.73% and 8.53% for 89 and 360 days, respectively. Meanwhile, the chemical inhibitor improved the velocity of contaminated concrete by 3.44%, 3.62, and 6.85% for 7, 89, and 360 days respectively. As a result, green and chemical inhibitors showed acceptable performance in improving the quality of concrete even in an extreme corrosive medium. However, *Areca catechu* showed better performance when compared to chemical inhibitor increased by the time.

3.3 Study on Hydration of Contaminated Concrete

Heat evolution of concrete is important mainly in casting mass concrete where cooling can cause cracking after a large temperature rise. The cement chemistry could provide an appropriate estimation of total heat of hydration per unit weight of Portland cement. The total heat of hydration of the cement at complete hydration H_{hyd} can be measured using Eq. (7) [24]:

$$H_{hyd} = 500p_{C3Sb} + 260p_{C2S} + 866p_{C3A} + 420p_{C4AF} + 624p_{SO3} + 1186p_{FreeCaO} + 850p_{MgO} \tag{7}$$

where H_{hyd} is total heat of hydration of the cement (J/g), and p_i is weight ratio of i -th compound in terms of the total cement content [24]. The heat of hydration of OPC, MN5C, CI2C, and GI2C mix investigated are depicted in Table 2.

Table 2 The details for Heat of hydration of all types of mix

Type of concrete	OPC	MN5C	CI2C	GI2C
Max.Temp (°C)	51.4	54.7	52.8	51.4
Initial Temp (°C)	28.5	29.2	29.3	29.3
Time to Max. Temp (hr)	10	10	10	12

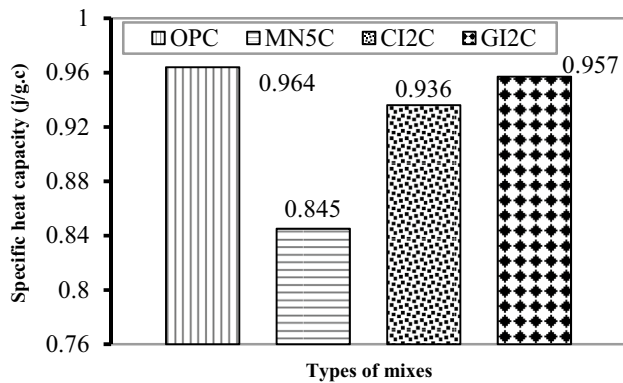


Fig. 3 Specific heat capacity values for all types mix

Similarly, all mixes showed approximately similar behavior in terms of heat evolution. Before a relatively steady state was attained during the period of study, all mix samples ultimately showed a gradual drop in temperature. This is similar to the results reported by other researchers [41, 49]. As expected, there was no significant difference in the peak temperature for green and chemical inhibitor-added concrete when compared to contaminated concrete sample. However, for chemical and green inhibitor-modified concrete, the peak temperatures were also lower than the contaminated concrete. The values for decreasing the peak temperature were 3.47% and 6.03% for green and chemical inhibitor-added concrete samples, respectively. Interestingly, addition of green inhibitor caused the peak temperature of contaminated concrete to decrease until it reached the same value with OPC. The

number of cracks that usually occurs due to the high heat of hydration during casting and hydration process could be decreased by increase in the peak temperature of cement hydration.

3.4 Specific Heat Capacity Investigation

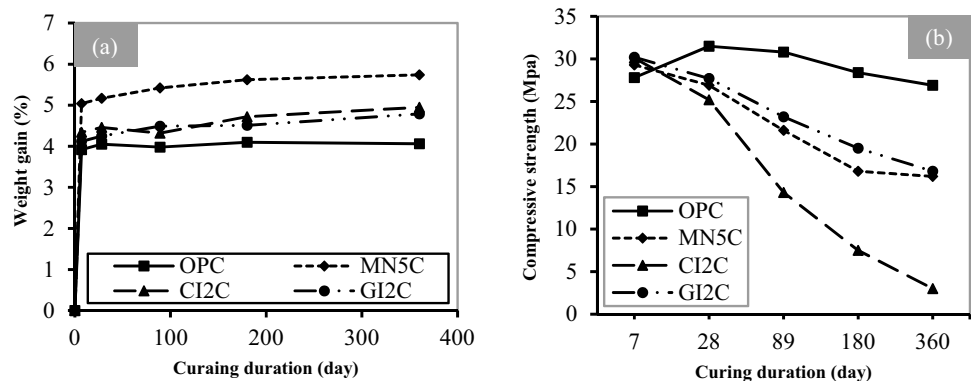
Specific heat capacity of solids is greater than fluids and similarly the fluids more than gases. This is justified by the molecular-kinetic theory. High-speed motion of molecules in gases with a little change in temperature increases the volume of the gas. In the case of solids, they need higher thermal energy to increase volume-specific heat capacity when compared to liquids [39, 50]. The thermal capacities of all types of concrete mixes are presented in Fig. 3.

The higher value of specific heat capacity for inhibitor-added samples depicted the better quality of concrete and fewer pores were available as a result of inhibitor addition. The green and chemical inhibitor-added samples could improve the specific heat capacity behavior of contaminated concrete by 10.77% and 13.25%, respectively.

3.5 Sulfate Resistance Behaviour

Depending on the type of sulfate existing in solution, it is supposed to attack calcium hydroxide, calcium aluminate hydrate, and calcium silicate hydrate. As illustrated in Fig. 4a, the initial weight gain of samples due to the absorption of the solution by the samples increased up to 28 days with recorded percentage. No significant increases were achieved with all samples after 28 days, which is similar to the results reported by another report [51]. As expected, contaminated samples showed the highest weight loss among all samples. This could be attributed to the sodium sulfate solution penetration and deterioration effect of sulfate on the samples. The graphical presentation of effect of sodium sulfate solution on compressive strength loss is depicted by Fig. 4b. The compressive strength of all samples decreased after 28 days. The compressive strength

Fig. 4 a weight gain and b compressive strength of all types of mix immersed in 5% Na₂SO₄

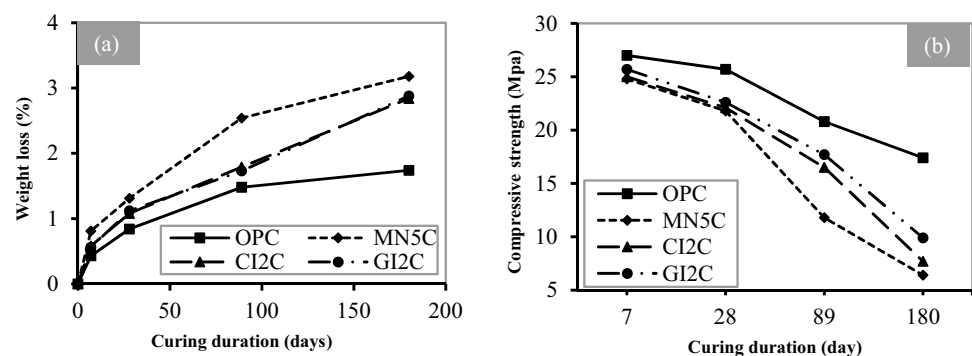


of ordinary concrete increased after 28 days. However, they showed slight decrease after 28 days. Those samples modified with chemical inhibitor showed an enormous strength loss. However, green inhibitor-added concrete still showed acceptable performance against sulfate attack. *Areca catechu* as green inhibitor slightly improved the compressive strength of contaminated samples. The values of compressive strength improvement by green inhibitor addition were 3%, 3%, 7.4%, and 16% and 3.7% for 7, 28, 89, 180, and 360 days, respectively, as green inhibitor showed its highest efficiency at 180 days.

3.6 Resistance to Acid Attack

The main sources for chloride ions could be found in marine environments and in deicing salts, admixtures containing chlorides and chloride-contaminated aggregates, cements, and polluted water. Wetting and drying of concrete accelerates the chloride ingress [52, 53]. Figure 5a shows the weight loss approach of immersed samples of all types of mix. As expected, the results depicted that contaminated samples showed the highest weight loss among all samples. This could be attributed to the porous structure of contaminated samples. The mass loss of OPC specimen in acidic medium can be explained by the direct attack on the aluminosilicate framework and the breakage of the Si–O–Al bonds [54, 55]. As shown in Fig. 5b, all samples reduced in compressive strength after the period of immersion. Those contaminated samples showed an enormous strength loss, it is absolutely due to the detrimental effect of magnesium sulfate and sodium chloride on microstructure of samples during the immersion period. Chemical and green inhibitors slightly improved the compressive strength of contaminated samples. An important implication of these findings is that the efficiency of green and chemical inhibitors on acid attack resistance increased by time. This fact could be a step forward in order to use the mentioned inhibitor in concrete. The inhibition efficiency of *Areca catechu* was found to be about 35% at 180 days obtained in terms of acid attack.

Fig. 5 a Weight loss and b Residual compressive strength of specimens immersed in 5% HCL



3.7 Corrosion Potential Analysis

Therefore, potential of corrosion was expected to increase even for OPC. The present study depicts that 2% of inhibitor could act as adequate proportion added in concrete to provide the highest inhibition efficiency. Corrosion potential of above -350 mV were recorded for all the exposure periods. *Areca catechu* inhibitor-added concrete was more corrosion resistant when compared with sodium nitrite. This might be due to its pore-blocking effects of green inhibitors. It is evident from the potential results of both chemical and green inhibitors that their inhibitions were acceptable for contaminated concrete samples as shown in Fig. 6a. *Areca catechu* could improve the corrosion resistance of contaminated concrete (Fig. 6b). The potential values tended to increase with increasing periods of exposure (become more negative). These results are in agreement with those reported by earlier research [56]. This is due to contamination of the concrete that corresponds to the compressive strength values recorded. R_c is considered as high resistance if the value is greater than 4 K Ω [57]. However, *Areca catechu* inhibitor was more resistant compared to sodium nitrite as represented in Fig. 6c. *Areca catechu* could decrease the corrosion rate of contaminated concrete about 30% even in an excessive harsh environment applied in the current research.

3.8 Linear Polarization Resistance

The corrosion rate of reinforced steel at the point of voltage measurement, and changes frequently over time could be directly achieved by measuring LPR's corrosion current density (I_{corr}) values [58]. The borderlines between passive and active corrosion were supposed to be from 0.1 to 0.5 $\mu\text{A}/\text{cm}^2$ [59]. The addition of chloride found decreases the polarization resistance, which results in the increase in current density as shown in Fig. 7a. The competition between the aggressive chloride ions and the passivating hydroxyl ions results in decreasing the polarization resistance. Chloride ions are expected to react with hydrated tricalcium aluminate (C_3A) hydrate to form chloroaluminate

Fig. 6 **a** Corrosion potential, **b** Corrosion rate, and **c** Concrete resistance as a function of exposure time

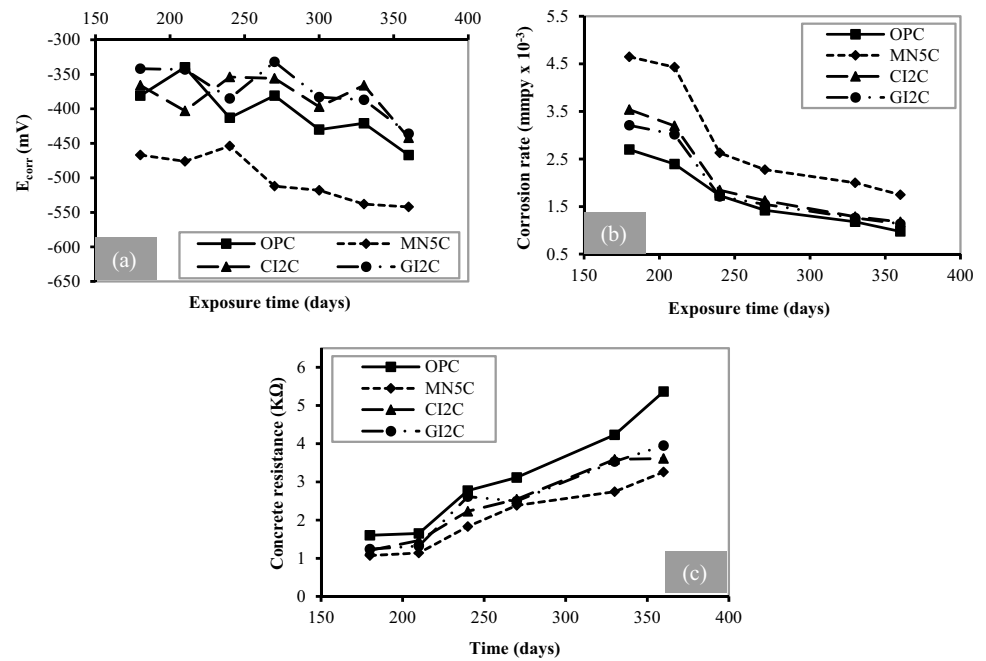
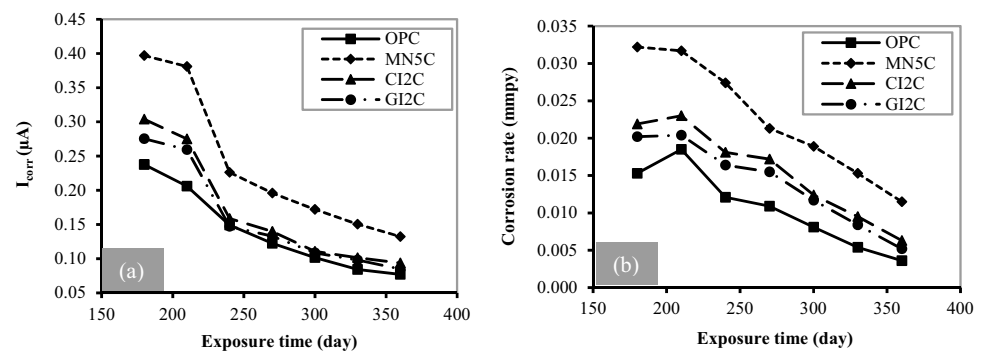


Fig. 7 **a** Current density and **b** Corrosion rate of concrete as a function of exposure time



($C_3A \cdot CaCl_2 \cdot 10H_2O$) that may contain 75–90% chloride. Chemical and green inhibitors showed similar performance in reducing the current density that leads to corrosion rate reduction regarding Fig. 7b.

As calculated from the data represented in Fig. 7, the green inhibitor decreased the corrosion current density (I_{corr}) by 30% that shows the high inhibition efficiency of *Areca catechu* as a green corrosion inhibitor. The cathodic and anodic Tafel slopes, corrosion potential, and the values of corrosion current are achieved by the anodic and cathodic regions of the Tafel plots. Extrapolating the Tafel lines to the corrosion potential could result in corrosion current density (I_{corr}). The variation of potential depicted as a function of current density is shown in Fig. 8a and b. It is clear that the presence of green and chemical inhibitors shifted both anodic and cathodic curves to lower current densities for all the exposure times. Inhibitors could be known as anodic or cathodic type when the change in

E_{corr} is larger than 85 mV. The largest displacement in this research was exhibited by *Areca catechu* extract at 53 mV. Thus, it may be concluded that *Areca catechu* extract acted as a mixed-type inhibitor. The corrosion propagation approach and structure deterioration increase by time. This is in agreement with another research done before [60].

3.9 Actual Corrosion Rate

There is an increasing trend in weight loss by time. This is attributed to the contamination of specimen using sodium chloride and magnesium sulfate. The weight loss increase in OPC sample was due to the wet and dry cycle accompanied by sea water utilization as curing medium that resulted in increasing the chloride penetration to the concrete. Weight loss and corrosion rate values decreased by time using Sodium nitrite and *Areca catechu* as chemical and green inhibitors, respectively, and represented in Fig. 9a and b.

Areca catechu caused reduction in weight loss of contaminated concrete 51.4% at 360 days. In addition, sodium nitrite could decrease the weight loss of contaminated concrete samples by 45.6% for the respective duration similar to the green inhibitor. This is approved by findings represented in many researches [45, 61–64]. Visual observations for corrosion propagation of steel reinforcement in contaminated and inhibitors-added concrete are represented in Fig. 10. From the figure, it is clearly evident that the corrosion product is more produced in contaminated concrete when compared to ordinary and inhibitor-added concrete. It is due to the deterioration of corrosive compounds added. The inhibitory effect of *Areca catechu* added as green inhibitor could be significantly visible.

3.10 Discussions on Microstructure Analysis

Reduction in the alkalinity of the concrete caused by $Mg(OH)_2$ releases more Ca^{2+} through C–S–H, so that it increases the formation of gypsum and lastly decomposing C–S–H to non-cementitious compounds of MSH. The effect of Mg^{2+} on concrete could be described using Eq. (8):



A denser structure can be seen in the morphology of the inhibitor-added concrete. Rougher and denser surface confirms the higher compressive strength and higher modulus elasticity that shows strong bonding between cement particles as confirmed by the compressive strength and modulus elasticity results for *Areca catechu*-added samples. This hydration product reacts with pozzolan to form more

Fig. 8 Corrosion potential of all mixes at **a** 180 days, **b** 360 days

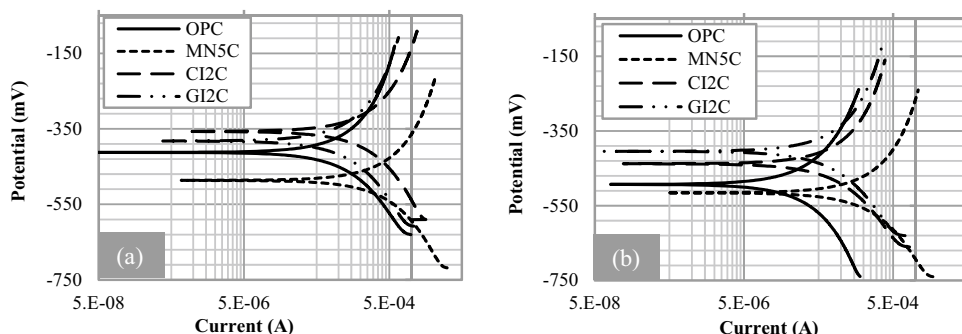


Fig. 9 **a** Weight loss and **b** corrosion rate of all mixes as a function of exposure time

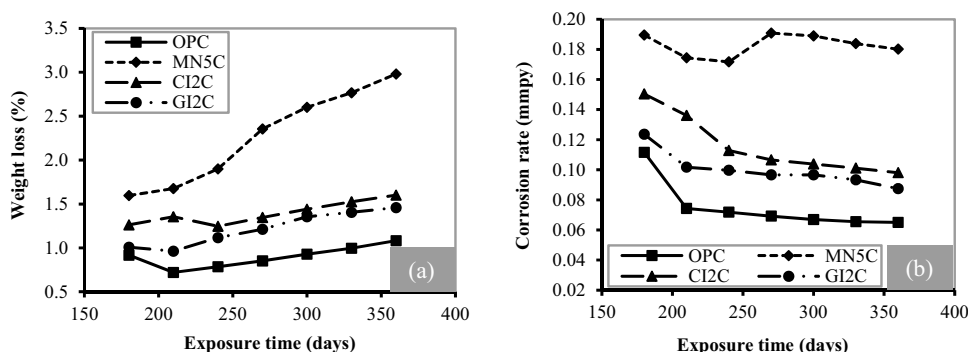
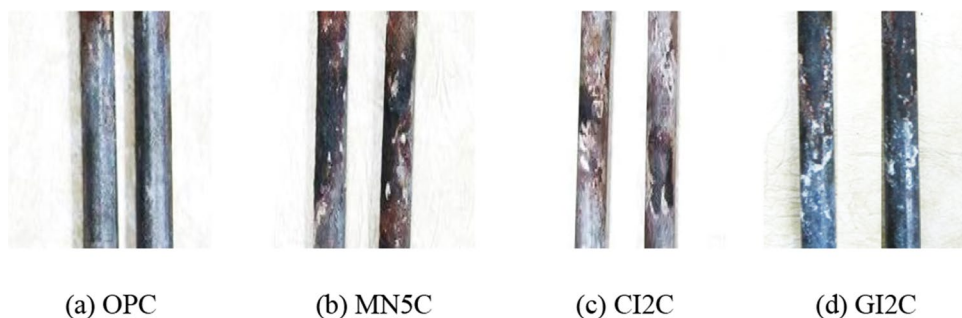
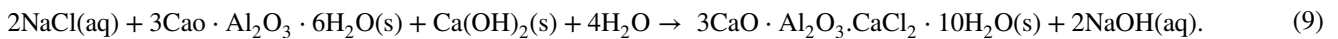


Fig. 10 Visual observation for specimen at 270 days, **a** OPC, **b** MN5C, **c** CI2C, **d** GI2C



C–S–H gel, producing a denser structure. Compared with the OPC and Contaminated concrete sample, inhibited samples had relatively more homogeneous surfaces and exhibited a smoother structure with some micro cracks but few air voids at the steel surface which explained the good inhibition performances of both chemical and green inhibitors [65–67]. The dense microstructure of chemical and green-inhibited samples accompanied by the presence of visible micro cracks might suggest the pore-blocking role played by sodium nitrite and *Areca catechu* as clearly shown in Figs. 11 and 12. The most prominent factor which influences the natural corrosion reinforcement in concrete is dissolved oxygen. Reinforced corrosion is proportional to oxygen content in the system [6]. The level of oxygen for OPC, contaminated concrete, and chemical inhibited sample was high compared to the *Areca catechu*-added sample, which surprisingly decreased the dissolved oxygen according to the results derived from EDX tests as presented in Table 3.

According to Asipita et al. [57], the C–S–H interacted with the crystal of NaCl showing ettringite as the white background suggesting a possible formation of Friedel's salt under chloride ingress. When free tricalcium aluminate (C_3A) comes in contact with sodium chloride, it will result in Friedel's salt formation as reported by Koleva et al. [68]. The mentioned reaction is as shown in Eq. (9):



Therefore, to compensate the destructive effect of above reaction, addition of inhibitors is considered. Inhibitors are supposed to boost the cations at the interfacial transition zones (ITZ) between aggregates and cement paste to improve the detrimental effects of ettringite and Friedel's salt formations [57]. Figure 11d showed no visible traces of crack and ettringite formation. This might be attributed to higher silicon content that buffers C–S–H phases which probably converted virtually all the portlandite.

3.11 Inhibition Mechanism

The performance of an organic inhibitor is related to the chemical structure and physicochemical properties of compound like functional groups, electron density, p -orbital character, and the electronic structure of the molecule. Inhibitory effect of natural corrosion inhibitors clearly evidenced the adsorption process involved during metal. Thus, the green inhibitors protect metal through adsorption mechanism which is found to follow Langmuir adsorption isotherm. Corrosion inhibition of *Areca catechu* (Areca Palm) is probably based on molecule adsorption. The molecules can adsorb on the metal surface by displacing water molecules on the surface and form a compact barrier.

Fig. 11 Gypsum formation in **a** MN5C, **b** MN5C, **c** CI2C, **d** GI2C concrete at 180 days

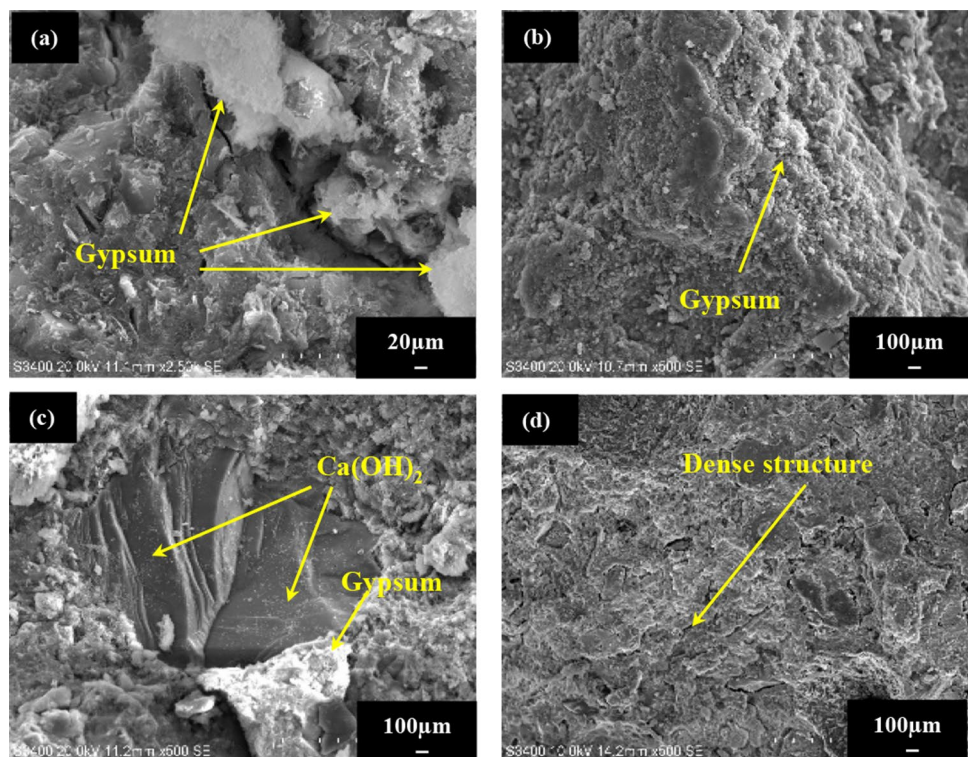


Fig. 12 Effect of inhibitor on steel in **a** MN5C, **b** MN5C, **c** CI2C, **d** GI2C at 360 days

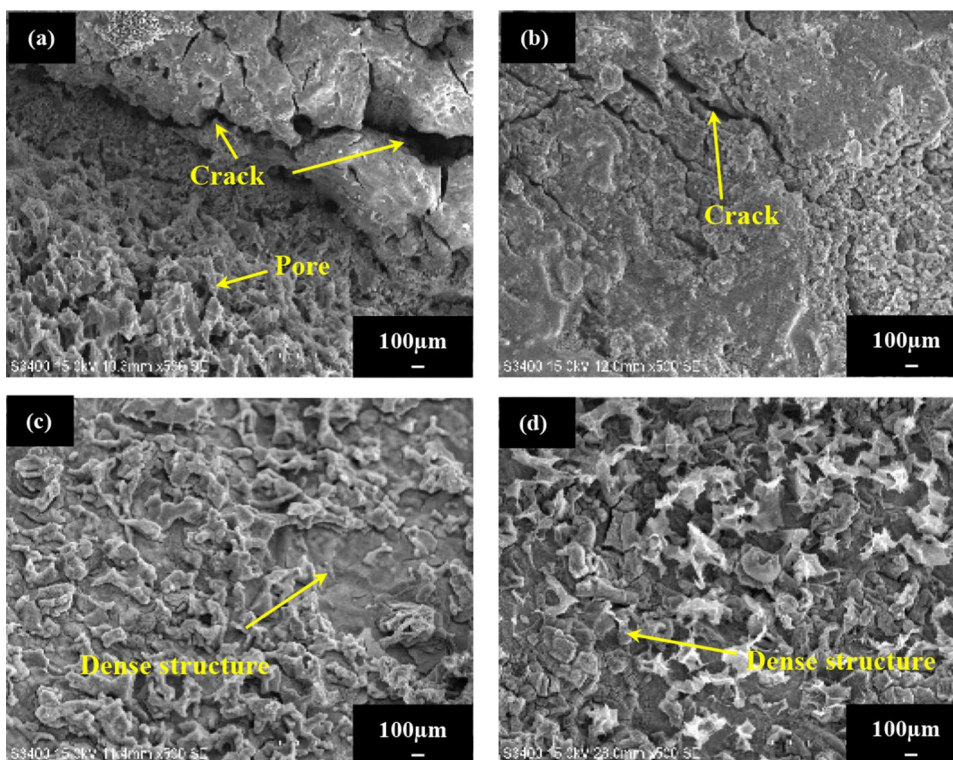


Table 3 Oxygen level of all samples of steel at 180 and 360 days

Duration	OPC	MN5C	CI2C	GI2C
180 D	19.97	26.72	22.96	10.24
360 D	23.94	30.87	23.94	7.65

The compound inhibits corrosion by controlling both the anodic and cathodic reactions as *Areca catechu* leaf extract proved to be a mixed-type corrosion inhibitor in Sect. 3.8. Availability of no-bonded (lone pair) and π -electrons in inhibitor molecules facilitates electron transfer from the inhibitor to the metal according to what earlier researchers reported [69, 45]. On the other hand, the effect of Mg^{2+} on concrete could be described using following Eq. (10):



High amount of alkali compounds is needed to compensate the detrimental effect of Mg^{2+} as mentioned in Eq. (10), and also for the pore solution to be absorbed onto the surface of steel reinforcement in concrete. Hence, introduction of inhibitors could be an effective method to compensate the effect of gypsum formation at the mutual zone between concrete and steel reinforcement (ITZ) [57]. The inhibitors considered to boost the cations amount at interfacial transition zone (ITZ) due to their alkalinity as proved for *Areca catechu* in the current study by application of AAS

test. Addition of inhibitors could also enhance the cement hydration due to curing process inside the concrete which leads to reducing the capillary pores. It is the high level of potassium and sodium from the inhibitor which combined with hydroxide and maintained the pH between 12 and 13. Passivating the steel and forming a dense gamma ferric oxide that is self-maintaining and preventing rapid corrosion is a result of the mentioned high level of alkalinity. *Areca catechu* which contains high potassium of 11,720 ppm as an alkaloid is responsible for the adsorption. Alkaloids are a group of nitrogen-containing bases in heteroatom's compounds.

4 Conclusions

In this study, *Areca catechu* leaf extract has been utilized in order to inhibit the corrosion of reinforcement in concrete. Moreover, the effect of mentioned green corrosion inhibitor on concrete properties was investigated. On the basis of the performed test, the following conclusions were drawn from this study:

- *Areca catechu* inhibitor was more resistant to corrosive medium compared to sodium nitrite. The mentioned issue could be done through its pore-blocking characteristics, so that it can prevent the formation of discrepancy

eration of cells, which promote corrosion on the steel surface due to oxygen level.

- Sodium nitrite and *Areca catechu* significantly decreased the corrosion rate of contaminated concrete samples. *Areca catechu*-added sample revealed a dense texture-clustered formation of gypsum. However, there is no gypsum visible in SEM observation for *Areca catechu*-added concrete. Addition of *Areca catechu* to the concrete showed a rougher surface compared to other samples at 360 days.
- *Areca catechu* showed superior performance in terms of heat evolution when compared to sodium nitrite as chemical inhibitor. The higher value of specific heat capacity for inhibitor-added samples depicted the better quality of concrete and fewer pores.

Acknowledgements The authors would like to dedicate the acknowledgement of gratitude to Ministry of Education Malaysia for the financial support Grant No: 4S090. Technical staffs from department of structure and materials, Faculty of Civil Engineering, RMC UTM and Institute of bio-product and development of UTM are also appreciated.

Compliance with Ethical Standards

Conflict of interest On behalf of all authors, the corresponding author declares that there is no conflict of interest that could have appeared to influence the work reported in this paper.

References

1. Abdulsada SA, Al-mosawi AI, Hadi AAA (2017) Waste plants as a green inhibitor for reinforced concrete. *Recent Trends Civil Eng Technol* 7(3):53–58
2. Edoziuno FO, Odoni BU, Adediran AA (2019) Analyses of the gravimetric and electrochemical effects of C16H13N3O3 on mild steel corrosion in 0.5 M H₂SO₄. *J Phys* 1378:1–11
3. Golewski GL (2018) Evaluation of morphology and size of cracks of the interfacial transition zone (ITZ) in concrete containing fly ash. *J Hazard Mater* 18:1–29
4. Guo B, Wang X, Wang Y, Shao Y (2019) Study on the forecasting of the hot corrosion resistance of typical superalloys for aeroengines. *J Mater Sci Eng* 685:1–7
5. Ja M, Ja T (2017) Evaluation of maximum and minimum corrosion rate of steel rebars in concrete structures, based on laboratory measurements on drilled cores. *Procedia Eng* 193:486–493
6. Jiang S, Gao S, Jiang L, Guo M, Jiang Y, Chen C, Jin M (2018) Effects of deoxyribonucleic acid on cement paste properties and chloride- induced corrosion of reinforcing steel in cement mortars. *Cement Concr Compos* 91:87–96
7. Kharismadewi D, Yuliwati E (2020) Wuluh starfruit (*Averrhoa bilimbi* linn.) leaves extract as green corrosion inhibitor in reinforced steel. *J Phys* 1444:1–7
8. Liu J, Ou G, Qiu Q, Chen X, Hong J, Xing F (2017) Chloride transport and microstructure of concrete with / without fly ash under atmospheric chloride condition. *Constr Build Mater* 146:493–501
9. Liu J, Qiu Q, Chen X, Xing F, Han N, He Y, Ma Y (2017) Understanding the interacted mechanism between carbonation and chloride aerosol attack in ordinary Portland cement concrete. *Cem Concr Res* 95:217–225
10. Liu Z, Song N, Wang Z (2017) Properties and characterization on a novel aqueous inhibitor for inhibiting alloy steel corrosion in chloride solution. *J Mater Civ Eng* 29(9):1–6
11. Wu Q, Li X, Xu J, Wang G, Shi W, Wang S (2019) Size distribution model and development two curing methods. *Materials* 12:1846
12. Pradipta I, Kong D, Ban J, Tan L (2019) Natural organic antioxidants from green tea form a protective layer to inhibit corrosion of steel reinforcing bars embedded in mortar. *Constr Build Mater* 221:351–362
13. Wu X, Li L, Li H, Li B, Ling Z (2018) Effect of strain level on corrosion of stainless steel bar. *Constr Build Mater* 163:189–199
14. Zhu W, François R, Sun C, Dai J (2017) Influences of corrosion degree and corrosion morphology on the ductility of steel reinforcement. *Constr Build Mater* 148:297–306
15. Fernandez I, Lundgren K, Zandi K (2018) Evaluation of corrosion level of naturally corroded bars using different cleaning methods, computed tomography, and 3D optical scanning. *Mater Struct* 51(3):1–13
16. Hussain RR (2011) Effect of moisture variation on oxygen consumption rate of corroding steel in chloride contaminated concrete. *Cement Concr Compos* 33(1):154–161
17. Gavela S, Ntziouni A, Rakanta E, Kouloumbi N, Kasselouri-Rigopoulou V (2013) Corrosion behaviour of steel rebars in reinforced concrete containing thermoplastic wastes as aggregates. *Constr Build Mater* 41:419–426
18. Wang Z, Zeng Q, Wang L, Yao Y, Li K (2014) Corrosion of rebar in concrete under cyclic freeze-thaw and Chloride salt action. *Constr Build Mater* 53:40–47
19. Castela AS, Da Fonseca BS, Duarte RG, Neves R, Montemor MF (2014) Influence of unsupported concrete media in corrosion assessment for steel reinforcing concrete by electrochemical impedance spectroscopy. *Electrochim Acta* 124:52–60
20. Rakanta E, Zafeiropoulou T, Batis G (2013) Corrosion protection of steel with DMEA-based organic inhibitor. *Constr Build Mater* 44:507–513
21. Fei FL, Hu J, Wei JX, Yu QJ, Chen ZS (2014) Corrosion performance of steel reinforcement in simulated concrete pore solutions in the presence of imidazoline quaternary ammonium salt corrosion inhibitor. *Constr Build Mater* 70:43–53
22. Palanisamy SP, Maheswaran G, Kamal C, Venkatesh G (2016) *Prosopis juliflora*—A green corrosion inhibitor. *Res Chem Intermed* 42:1–18
23. Rani BEA, Basu BBJ (2012) Green inhibitors for corrosion protection of metals and alloys: an overview. *Int J Corros* 12(1):1–15
24. Sangeetha M, Rajendran S, Sathiyabama J, Krishnaveni A, Shanthi P, Manimaran N, Shyamaladevi B (2011) Corrosion inhibition by an aqueous extract of phyllanthus amarus. *Portugaliae Electrochimica Acta* 29(6):429–444
25. Shahid M (2011) Corrosion protection with eco-friendly inhibitors. *Adv Nat Sci* 2(4):1–6
26. Shainy KM, Rugmini AP, Unni KN, Benjamin S, Joseph A (2016) Surface interaction and corrosion inhibition of mild steel in hydrochloric acid using pyoverdine, an eco-friendly bio-molecule. *J Bio Tribo Corros* 2(20):1–12
27. Fouda AS, ShalabiHossiany KA (2016) Moxifloxacin antibiotic as green corrosion inhibitor for carbon steel in 1 M HCl. *J Bio Tribo Corros* 2(18):1–13
28. Qiao G, Guo B, Ou J, Xu F, Li Z (2016) Numerical optimization of an impressed current cathodic protection system for reinforced concrete structures. *Constr Build Mater* 119:260–267
29. Khan M, Ali M (2016) Use of glass and nylon fibers in concrete for controlling early age micro cracking in bridge decks. *Constr Build Mater* 125:800–808

30. Magie SJH, Subhashini JS, Arulraj J (2020) *Sunova spirulina* powder as an effective environmentally friendly corrosion inhibitor for mild steel in acid medium. *J Bio- Tribo-Corros* 6(71):1–13
31. Torres-Acosta AA (2007) *Opuntia-Ficus-Indica* (Nopal) mucilage as a steel corrosion inhibitor in alkaline media. *J Appl Electrochem* 37(7):835–841
32. Abdallah M, Altass HM, Jahdaly BAAL, Salem MM, Altass HM, Jahdaly BAAL, Some MMS (2018) Green chemistry letters and reviews some natural aqueous extracts of plants as green inhibitor for carbon steel corrosion in 0.5 M sulfuric acid. *Green Chem Lett Rev* 11(3):189–196
33. Alfakeer M, Abdallah M, Fawzy A (2020) Corrosion inhibition effect of expired ampicillin and flucloxacillin drugs for mild steel in aqueous acidic medium. *Int J Electrochem Sci* 15:3283–3297
34. Fawzy A, Abdallah M, Zafarany IA, Ahmed SA, Althaga II (2018) Thermodynamic, kinetic and mechanistic approach to the corrosion inhibition of carbon steel by new synthesized amino acids-based surfactants as green inhibitors in neutral and alkaline aqueous media. *J Mol Liquids* 265:276–291
35. Raghavendra N, Bhat JI (2018) Anti-corrosion properties of *Areca palm* leaf extract on aluminium in 0.5 M HCl environment. *South Afr J Chem* 71(2018):30–38
36. Dang VH, Francois R (2013) Influence of long-term corrosion in chloride environment on mechanical behaviour of RC beam. *Eng Struct* 48:558–568
37. Elfordy S, Lucas F, Tancret F, Scudeller Y, Goudet L (2008) Mechanical and thermal properties of lime and hemp concrete (hemcrete) manufactured by a projection process. *Constr Build Mater* 22:2116–2123
38. Edvard A, Deherde A (2016) Hygrothermal performance of lime – hemp wall assemblies. *J Building Phys* 34(1):5–25
39. Walker R, Pavia S (2014) Moisture transfer and thermal properties of hemp-lime concretes. *Constr Build Mater* 64:270–276
40. Chandara C, Mohd Azizli KA, Ahmad ZA, Saiyid Hashim SF, Sakai E (2012) Heat of hydration of blended cement containing treated ground palm oil fuel ash. *Constr Build Mater* 27(1):78–81
41. Monder M, Samia B, Toufik C, Nabila C (2019) Inhibition efficiency of cinnamon oil as a green corrosion inhibitor. *J Bio-Tribo-Corros* 5(28):1–9
42. Saxena A, Kumar J (2020) Phytochemical screening, metal binding studies and applications of floral extract of *Sonchus oleraceus* as a corrosion inhibitor. *J Bio- and Tribo-Corros* 6(55):1–10
43. ASTM C 109 (1981) Test method for compressive strength of hydraulic cement mortars. Annual book of ASTM standards, American Society for Testing and Materials, Philadelphia, USA
44. Karthick SP, Muralidharan S, Saraswathy V, Thangavel K (2014) Long-term relative performance of embedded sensor and surface mounted electrode for corrosion monitoring of steel in concrete structures. *Sens Actuators B* 192:303–309
45. Zhao XD, Yang J, Fan XQ (2010) Review on research and progress of corrosion inhibitors. *Appl Mech Mater* 44–47:4063–4066
46. ASTM G1 (2003) Standard practice for preparing, cleaning, and evaluating corrosion test specimens, Annual book of ASTM standards, American Society for Testing and Materials, Philadelphia, USA
47. Madandoust R, Mousavi SY (2012) Fresh and hardened properties of self-compacting concrete containing metakaolin. *Constr Build Mater* 35:752–760
48. Girardi F, Maggio RD (2011) Resistance of concrete mixtures to cyclic sulfuric acid exposure and mixed sulfates: effect of the type of aggregate. *Cement Concr Compos* 33(2):276–285
49. Mehmannaavaz T, Ismail M, Sumadi SR, Bhutta MAR, Samadi M, Sajjadi SM (2014) Binary effect of fly ash and palm oil fuel ash on heat of hydration aerated concrete. *Sci World J*. <https://doi.org/10.1155/2014/461241>
50. Pomianowski M, Heiselberg P, Jensen RL, Cheng R, Zhang Y (2014) A new experimental method to determine specific heat capacity of inhomogeneous concrete material with incorporated microencapsulated-PCM. *Cem Concr Res* 55:22–34
51. Yusuf OT (2015) Effects of palm oil fuel ash and metakaolin blend on properties of geopolymer mortar. Doctor Philosophy, Universiti teknologi malaysia, Skudai
52. Bonić Z, Čurčić GT, Davidović N, Savić J (2015) Damage of concrete and reinforcement of reinforced-concrete foundations caused by environmental effects. *Procedia Eng* 117(1):416–423
53. Çullu M, Arslan M (2014) The effects of chemical attacks on physical and mechanical properties of concrete produced under cold weather condition. *Constr Build Mater* 50:202–209
54. Angst U (2011) Chloride induced reinforcement corrosion in concrete - Concept of critical chloride content – methods and mechanism, Concept of Critical Chloride Content. Doctor Philosophy, Norwegian university of technology and science, Trondheim
55. Shah N, Shah H, Shah D, Patel VN (2014) A review on compressive and tensile strength of concrete containing rice husk ash and coir fiber. *Sch J Eng Technol* 2:750–754
56. Gerengi H, Kocak Y, Jazdzewska A, Kurtay M, Durgun H (2013) Electrochemical investigations on the corrosion behaviour of reinforcing steel in diatomite- and zeolite-containing concrete exposed to sulphuric acid. *Constr Build Mater* 49:471–477
57. Asipita SA, Ismail M, Majid MZA, Majid ZA, Abdullah C, Mirza J (2014) Green *Bambusa Arundinacea* leaves extract as a sustainable corrosion inhibitor in steel reinforced concrete. *J Clean Prod* 67:139–146
58. Alghamdi SA, Ahmad S (2014) Service life prediction of RC structures based on correlation between electrochemical and gravimetric reinforcement corrosion rates. *Cement Concr Compos* 47:64–68
59. Królikowska A, Kuziak J (2011) Impedance study on calcium nitrite as a penetrating corrosion inhibitor for steel in concrete. *Electrochim Acta* 56(23):7845–7853
60. Güneyisi E, Gesoğlu M, Karaboğa F, Mermerdağ K (2013) Corrosion behavior of reinforcing steel embedded in chloride contaminated concretes with and without metakaolin. *Compos B Eng* 45(1):1288–1295
61. Abdel-Gaber AM, Khamis E, Hefnawy A (2011) Utilizing *Arghel* extract as corrosion inhibitor for reinforced steel in concrete. *Mater Corros* 62(12):1159–1162
62. Esah H, Chukwuekezie C, Idris J, Mohammad I (2013) Effect of green inhibitor on the corrosion behaviour of reinforced carbon steel in concrete. *ARN J Eng Appl Sci* 8(5):326–332
63. Quraishi MA, Kumar V, Abhilash PP, Singh BN (2011) Calcium stearate: a green corrosion inhibitor for steel in concrete environment. *J Mater Environ Sci* 2(4):365–372
64. Zekos I, McmeeKin K, Stack MM (2020) On the effect of pre-formed scales in mitigating corrosion of steels in CO₂ environments. *J Bio- Tribo-Corros* 6(2):1–12
65. Ali M, Ismail M, Tahir M, Fahim G (2018) Enhanced corrosion resistance of reinforced concrete: role of emerging eco-friendly *Elaeis guineensis*/silver nanoparticles inhibitor. *Constr Build Mater* 188:555–568
66. Deng S, Li X (2012) Inhibition by *Jasminum nudiflorum* Lindl. leaves extract of the corrosion of aluminium in HCl solution. *Corros Sci* 64:253–262

67. Li X, Deng S, Xie X (2014) Experimental and theoretical study on corrosion inhibition of oxime compounds for aluminium in HCl solution. *Corros Sci* 81:162–175
68. Koleva DA, Hu J, Fraaij ALA, Vanbreugel K, Dewit JHW (2007) Microstructural analysis of plain and reinforced mortars under chloride-induced deterioration. *Cem Concr Res* 37:604–617
69. Mobin M, Rizvi M (2016) Inhibitory effect of xanthan gum and synergistic surfactant additives for mild steel corrosion in 1M HCl. *Carbohydr Polym* 136:384–393

Publisher's Note Springer Nature remains neutral with regard to jurisdictional claims in published maps and institutional affiliations.